

# RSC Advances



This is an *Accepted Manuscript*, which has been through the Royal Society of Chemistry peer review process and has been accepted for publication.

*Accepted Manuscripts* are published online shortly after acceptance, before technical editing, formatting and proof reading. Using this free service, authors can make their results available to the community, in citable form, before we publish the edited article. This *Accepted Manuscript* will be replaced by the edited, formatted and paginated article as soon as this is available.

You can find more information about *Accepted Manuscripts* in the [Information for Authors](#).

Please note that technical editing may introduce minor changes to the text and/or graphics, which may alter content. The journal's standard [Terms & Conditions](#) and the [Ethical guidelines](#) still apply. In no event shall the Royal Society of Chemistry be held responsible for any errors or omissions in this *Accepted Manuscript* or any consequences arising from the use of any information it contains.

## ARTICLE

www.rsc.org/

## Design of live biochip for *in situ* Nanotoxicology studies: a proof of concept

Schaack Béatrice<sup>a,b,c,d,\*</sup>, Liu Wei<sup>e,f,g</sup>, Thiéry Alain<sup>h,m</sup>, Auger Aurélien<sup>i</sup>, Jean-François Hochepeid<sup>j,k</sup>, Castellan Mathieu<sup>d</sup>, Ebel Christine<sup>a,b,c</sup>, Chaneac Corinne<sup>l,m</sup>, Achouak Wafa<sup>e,f,g,m</sup>

This paper highlights the way in which eukaryotic cell and bacteria based biochips are relevant for nanotoxicological risk evaluation. Here we define NP-biochips as formatted surfaces containing nanoparticles (NPs). They are simple devices which can easily be used to generate quantitative data expressing the effects of NPs on biological material in parallelized medium throughput assays. Firstly we dropped NPs and bacteria onto an agarose layer, using fluorescent bacteria in order to follow by imaging the effects of these NPs on bacterial growth. Secondly we embedded the targeted NPs at precise spot locations in a matrix on which eukaryotic cells can adhere, and followed cell growth. We used titanium dioxide as model NPs for the concept validation. Both types of NP-biochip are realized in order to pattern NPs in 50 or 100 dried 400  $\mu\text{m}$  diameter spots on a glass plate, with less than 0.3% variation in concentration between spots. For anatase  $\text{TiO}_2$  NPs, we were able to record a non-toxic effect by measuring bacteria or eukaryotic cell survival. NPs are not internalized in bacteria; we thus used hyperspectral imaging to observe NPs on their surfaces. In contrast, NPs translocate in eukaryotic cells so we used fluorescent  $\text{TiO}_2$  and quantum dots to verify that NPs migrate from the NP-biochip matrix into bronchial cells. In order to illustrate the release of NP from the chip into the cell, we present the dose-response curve in the case of a toxic rutile  $\text{TiO}_2$  NP. These devices prevent cell and bacteria suffocation that is often observed in standard assays in wells due to NP precipitation. We believe that these tests realized on gel coated biochip are a rather realistic model for NP exposure *in situ*, imitating bacterial growth in biofilms and eukaryotic cells in tissues.

### 1. Introduction

Over the last 20 years, titanium dioxide ( $\text{TiO}_2$ ), in particular in the form of anatase and rutile nanoparticles (NPs), has contributed to a revolution in several industrial fields such as renewable energy, sustainable housing, environmental remediation and cosmetics<sup>1, 2</sup>. Nanoscale rutile has larger absorbance properties when compared to nanoscale anatase, in particular for ultraviolet rays. It is thus favored for outdoor application, i.e. industrial paints and sunscreen formulation. A reduction of the rutile particle size has led to a transparent and more attractive texture for sunscreens<sup>3, 4</sup>. In contrast, due to its electronic properties, the anatase  $\text{TiO}_2$  form is more effective for the production of electron-hole pairs and the generation of reactive oxygen species (ROS) upon exposure to light. As a result, anatase is widely used in self-cleaning glass and solar panels, as well as water purification membrane components<sup>5</sup>. Nevertheless, because they generate different levels of oxidative stress, both anatase and rutile are considered as potential carcinogens, where humans are concerned, by the International Agency for Research on Cancer. The toxicity of these materials needs therefore to be studied. Owing to the widespread use of engineered nanomaterials and their potential release into the environment, surface waters, waste water treatment facilities and other environments, their potential for adversely affecting these

ecosystems also raises concern. Microorganisms are key players in the global bio-geochemical cycling of nutrients, organic matter decomposition and waste treatment. Any damage to these microorganisms by NPs may disturb these functional ecosystems<sup>4, 6</sup>.

In 2010, the production of nanoscale  $\text{TiO}_2$  was estimated to be 6.3% of the world's production of titanium dioxide and could be found in 59 registered daily life products<sup>7</sup>. In relation to the manipulation of these large quantities, numerous hazard assessments have already been performed in order to evaluate primary routes for human exposure to  $\text{TiO}_2$  NPs. Different experiments analyzed the penetration of  $\text{TiO}_2$  NPs through the stratum corneum by electron microscopy and concluded to no plausible effect of  $\text{TiO}_2$  NPs penetration through the human healthy skin. Nevertheless their entry was reported at hair wounds and UV damaged skin levels<sup>8, 9</sup>. Based on small animal toxicology data,  $\text{TiO}_2$  NPs were classified as "harmful" in literature<sup>1, 10</sup>. Genotoxic mechanisms associated with oxidative stress and/or inflammation, induced *in vitro* by  $\text{TiO}_2$  NPs, have already been linked to negative health effects *in vivo*, such as respiratory tract inflammation and cancer in rats<sup>11-14</sup>. Due to their size and their ability to aggregate, the action of NPs occurs primarily through their contact with cell membranes<sup>15, 16</sup>. In

*vitro*, disruption of eukaryotic cell membranes by TiO<sub>2</sub> NPs was described<sup>17, 18</sup>. The mechanism would be related to structural changes in protein and phospholipid molecular damages<sup>19</sup>. These effects are triggered by oxidative stress<sup>8, 17, 20</sup> leading to the activation of redox sensitive pathways. Apoptosis induction by TiO<sub>2</sub> NPs has already been described, and the target cell type has been shown as a critical determinant to intracellular response and the level of NPs cytotoxicity<sup>17</sup>. Regarding inflammation, stronger release of cytokine has been described for cells incubated in the presence of ultrafine TiO<sub>2</sub> NPs (20 to 80 nm mix), compared to fine (larger than 100 nm) particles<sup>20</sup>. Regarding bacteria, their photocatalytic inactivation by TiO<sub>2</sub> NPs is already used for antimicrobial purposes<sup>5</sup>. Impairment of cell membrane integrity - through ROS generation upon treatment with TiO<sub>2</sub> NPs - seems to be the major cause of bacterial death<sup>6, 21</sup>.

Risk assessments are now carried out in order to increase the information available and to allow better decision making in the choice between several TiO<sub>2</sub> NPs according to their toxicity. Currently TiO<sub>2</sub> NPs can be synthesized by various methods, including sol-gel, hydrothermal, combustion and gas-phase, leading not only to different properties but also different levels of toxicity<sup>10</sup>. A worldwide recommendation to limit the manufacture of TiO<sub>2</sub> NPs to safer products is likely to reduce the risks NPs pose to human and environmental health<sup>22</sup>. In order to select these products, technologies have to be developed so as to accelerate toxicity research on NPs through rapid *in vitro* high throughput screening on bacteria as well as on eukaryotic cells.

In this article, we describe and analyze two innovative biochips, called NP-biochips, allowing a medium throughput screening for NP *in vitro* toxicity. These devices prevent cell and bacteria suffocation under a NP precipitate that is often observed in standard assays. An interesting concept addressing this point was already described by Pelletier et al.<sup>23</sup>; the idea was to analyze NP effect on bacteria using disk diffusion tests, but it did not allow determining an accurate localization of the NPs and the bacterial culture on the same substrate. Therefore, for bacteriological assessment of NP risk, we have adapted an agarose coating method over a glass slide<sup>24</sup>, described for bacteria imaging, allowing the combined deposition of NPs and bacteria. This first biochip allows 50 parallelized assays. We used hyperspectral imaging on this NP-biochip to simultaneously visualize the relative localization of TiO<sub>2</sub> NPs and *Pseudomonas brassicacearum* bacteria, a Gamma-proteobacterium described as a major beneficial root-colonizing population of *Arabidopsis thaliana* and *Brassica napus*<sup>25, 26</sup>. The second biochip was inspired by the siRNA biochip described by Gidrol et al.<sup>27</sup>. It describes a eukaryotic cell-based assay performed over 100 NP spots formed in a commercial eukaryotic extracellular extract on which cell adhesion was obtained. Translocation of Rhodamine B - labeled TiO<sub>2</sub> or quantum dots (QDs) NPs through human bronchial epithelial cell membranes was evidenced by fluorescence imaging. The perspectives offered by the two NP-biochips are discussed.

A few years ago, we suggested using 100 nL drops, containing 100 cells, to miniaturize cultures on a cell-on-chip substrate. This tool was successful in producing data, in particular IC50 measurements, describing toxicities (TOXDROP project granted by the European commission in FP6 program) in accordance with standard published data<sup>28</sup>. We develop in the present article a new concept which we called the 'NP-biochip', allowing to

colocalize in an automated way, in 50 or 100 spots, eukaryotic or bacterial cells and NPs of various types and concentrations. The format of the two types of NP-biochip, the spot size of 400 μm diameter, and the 2 mm distance between spot centers, was designed for automatic image capture of the spots using a motorized microscope and avoiding cell confluence.

## 2. Method

### 2.1. NP-biochip design

To analyze the effect of several NPs differing in size, shape and concentration, on bacteria or eukaryotic cells, replicates need to be done on the same substrate. We chose to perform our NP-biochip on a glass plate, since it is a universal object displaying a 75 x 25 mm printable area. Multiple assays were carried out on this surface combining NPs and cell colocalization and incubation. The distance between two consecutive spot centers was set to 2 mm. We chose for each assay area a 400 μm diameter surface, as it can easily be imaged using the 20 × lens of microscope. It corresponds to the dispense of 8 nL, that were obtained through the addition of 20 consecutive drops of 400 pL using the Sciflexarrayer® piezo-dispenser equipped with an 80 μm diameter nozzle. The liquid to be spotted was held in 96 V-shaped well microplates in order to minimize the volume used. The spotting was verified by an active drop volume control analyzing the image of the drop before spotting (Scienion®'s software).

### 2.2. Bacteria NP-biochip

75 x 25 mm glass plates were coated with 400 μL medium containing 1% agarose (Euromedex®, France) and Tryptic Soy Broth (TSB) (Difco®, France) at 3 g/L, rather than the usual 30 g/L concentration in order to decrease the possibility of NP-protein interactions. This mix was named Tryptic Soy Agarose (TSA). The coated glass plates were then kept (for days) hydrated lying on 25 mL agar (15 g/L) in individual Petri dishes. We used *Pseudomonas brassicacearum* strain NFM421, tagged with either red or green fluorescent proteins (RFP and GFP, respectively)<sup>29</sup>. The TiO<sub>2</sub> NP solutions were sonicated for 30 s just before mixing, in order to prevent NP precipitation. A mix of bacteria and NP was prepared, composed of 5 μL of bacterial culture grown overnight in 3 g/L TSB medium (i.e. 520 +/- 110 bacteria), and 100 μL of 0 to 100 mg/L TiO<sub>2</sub> NP. Using the Sciflexarrayer® piezo-dispenser (Scienion®, Germany), we dispensed 20 successive 400 pL drops of this mix on each of the 50 spots of the TSA coated glass substrate, at precise locations (Fig. 1). At this stage, the NP-biochip can be stored for up to one month at 4°C before analysis. Bacteria were then grown for 48 h at 30 °C on the NP-biochip housed by the wet Petri dish mentioned above. The NP-biochip was examined using the Chemidoc® MP imager (Biorad®, USA) in order to quantify bacterial growth. For the purpose of microscopic analysis, the NP-biochip was mounted with a glass coverslip; measurements were made using an oil immersion 100 × magnifying lens. Hyperspectral image analyses were performed using Cytoviva® HSI (USA) system. Spectra were measured with the Specim V10E spectrometer (400–1000 nm). ENVI v.4.4 software was used to record the spectral image using mixture tuned matched filtering, in order to discriminate spatial distributions of NPs and bacteria. Images of bacteria and NPs on the spots, shown on Fig. 1a, e.g. anatase NP, were obtained using a fluorescence

microscope Nikon® 50i equipped with a fluorescent light and a 100 × magnifying lens. Transmission Electron Microscopy was carried out as described in Dessombz et al.<sup>30</sup>

### 2.3. Eukaryotic cell NP-biochip

16-HBE human bronchial epithelial cells were cultured as adherent monolayers in modified Eagle medium (MEM from Invitrogen-GIBCO®, USA) containing 10% heat-inactivated (56 °C, 30 minutes) fetal bovine serum (Dutscher®, France), 1 mM L-glutamine and 25 mM N-2-hydroxyethylpiperazine-N'-2-ethanesulfonic acid (HEPES, from Invitrogen-GIBCO®, USA), as described by Merendino et al.<sup>31</sup>. Hydrophobic glass substrates were prepared as in Azioune et al.<sup>32</sup>. Castel et al.<sup>33</sup> have shown that rehydration of cell biochip determines its sensitivity and fidelity. Therefore we have carefully followed the protocols of Pitaval et al.<sup>34</sup> and Azioune et al.<sup>32</sup> to modify the glass plates in order to allow matrix protein folding during rehydration. In order to form 400 μm wide dried spots containing NPs and extracellular matrix, we first mixed the NP at the desired concentration with 6% matrigel® (Invitrogen-GIBCO®, USA) over a 96 wells plate. Using the Sciflexarrayer® piezo-dispenser (Scienion®, Germany) we dispensed 20 successive drops of 400 pL of this solution (NP + matrigel® + H<sub>2</sub>O) on the hydrophobic glass substrate at precise locations (Fig. 3a). Particular attention was given to avoid TiO<sub>2</sub> precipitation using micropipetting and vigorous mixing before piezo dispensing. To allow a slow dehydration of the spots and to avoid the doughnut desiccation effect, the glass slides were kept at a temperature 2°C above the measured dew point during spotting. At this point, the NP-biochips were left to dry for 30 min, and stored in a dry atmosphere for up to one month. 16-HBE human epithelial bronchial cells were dispersed using trypsin in the culture medium. 10 mL containing one million cells was then added onto the chip lying at the bottom of a 9 cm wide Petri dish. After 10 min, the plate was washed twice with 10 mL cell-free medium to remove the non-attached cells. The whole device, with 10 mL medium, was then incubated for two days at 37 °C. Hoechst® 33342 was used to color the nucleus and Alexa Fluor® 488 phalloidin (Life Technologies®, USA) was used to color the actin network. We also used the fluorescent LIVE/DEAD® Cell Viability Assays (Life Technologies, USA) according to the manufacturer's instructions. For the purpose of microscopic analysis, the NP-biochip was mounted using VectorShield® resin and a glass coverslip. Microscope (Olympus® BX51) image captures were automatically obtained using Pathfinder OSA® Software (Imstar®, Paris). Nucleus labeling enabled easy quantification of cell per spot (i.e. 407 ± 57 cells).

### 2.4. NPs

TiO<sub>2</sub> NPs were anatase and rutile of various sizes and morphologies. The NPs used in Fig. 1a and Fig. 5a,b were anatase isotropic particles of 25 nm diameter and in Fig. 2a rutile nanorods of 100 nm x 12 x 12 nm. They were lab-made. Details of their synthesis, characteristics and preparation are available in<sup>30</sup>. The commercial anatase TiO<sub>2</sub> NPs used in Fig. 5c, e and f were from Alfa Aesar (anatase spheres of 23 nm diameter, and rutile sticks of 47x18x18nm). Rhodamine B labeled - TiO<sub>2</sub> NPs were used to observe translocation in eukaryotic cells as it appears in Fig. 3f and Fig. 4. They were manufactured using TiO<sub>2</sub> nanometric particles (Aeroxide® P25S Degussa commercialized by Evonik®, Germany) with a specific surface

area of 50 m<sup>2</sup>/g, mainly made up of spherical 25 nm diameter NPs and a mix of 70% anatase / 30% rutile. Tetrahydrofuran and rhodamine B were purchased from Sigma-Aldrich® (France) and used without further purification. Supercritical doping of nanometric TiO<sub>2</sub> powder was performed in a cylindrical high pressure autoclave. The reactor was first charged with 1 g of TiO<sub>2</sub> powder, 1 mL of tetrahydrofuran and 100 mg of Rhodamine B. CO<sub>2</sub> was then liquefied through a cooling unit (CF40 unit, JULABO®, Germany) and compressed by a PU-2088-CO<sub>2</sub> Plus pump (JASCO®, France) to 40 bars. The vessel was then heated up to 50 °C for 1 h using an electrical resistance and a pressure of 80 bars was reached (the critical point of CO<sub>2</sub> is 73 bars at 31 °C). After 1 h treatment, the vessel was cooled down to room temperature, and pressure was released. After opening the autoclave, the TiO<sub>2</sub> nanomaterial was recovered using purified water. The NPs were then washed twice by centrifugation at 8,000 rpm (10 min) with water. The recovered sample was dialyzed (3,500 MWCO, Roth®, France) in water for 1 week so as to remove any trace of free Rhodamine B. The preparation of 7 nm QDs of CdSe/CdS/ZnS is described in Protiere et al.<sup>35</sup>. They were spotted at 20 nM.

## 3. Results

### 3.1. Bacteria NP-biochip

The bacteria NP-biochip consisted in a glass plate coated with a solid phase containing the appropriate bacterial culture medium mixed with 1% agarose, on which 50 400 μm diameter individualized spots containing bacteria and NPs were deposited. *P. brassicacearum* is a Gram-negative bacteria plant root<sup>26</sup>, small enough to pass through the 80 μm wide piezo-dispenser nozzle. Therefore, on the NP-biochip, bacteria and NPs could be spotted together (Fig. 1a). The immobilization of the bacteria in each spot of the NP-biochip was obtained using a thin layer of TSA medium coating as described by de Jong et al.<sup>24</sup>. We succeeded in keeping the bacteria alive at 4°C by maintaining the NP-biochip hydrated in a wet Petri dish containing a bed of agar at 15 g/L. For investigating NP toxicity, bacteria and NPs were incubated at 30°C during 2 days. The use of fluorescent bacteria expressing GFP and RFP allowed quantification of their growth through microscope imaging, thus paving the way to the determination of NP toxic or non-toxic effect using fluorescence quantification (Fig. 1b and c)<sup>29</sup>. We first noticed (Fig. 1c, d and e) that bacteria as well as NPs were well distributed throughout the spots. Quantitative evidence can be observed in Fig. 5a where fluorescent bacteria growth on the NP-biochip was evaluated after 2 days using a fluorescence profile. The anatase NP was found as nontoxic up to 100 mg/L. It compares well to results obtained in classical 96 wells microtiter plates after 2 days' exposure to NPs, and recording bacterial numbers by serial dilution counting (Fig. 5b). The comparison of the amount of bacteria surviving in the presence of NPs, using either around 520 bacteria per spot on the chip or nearly a thousand bacteria per well, showed that this NP does not prevent bacterial division. In addition, thanks to the use of a novel methodology based on hyperspectral imaging with enhanced Dark field microscopy<sup>36</sup>,<sup>37</sup>, co-localization of bacteria and NPs was made possible, where fluorescent bacteria and TiO<sub>2</sub> NPs are simultaneously detected, as illustrated in Fig. 1d and 1e. NPs appear as very bright dots, since under enhanced dark field conditions, particles appear 150 fold brighter than under conventional dark field microscopy due to Köhler illumination by collimated light source at oblique angles.

## ARTICLE

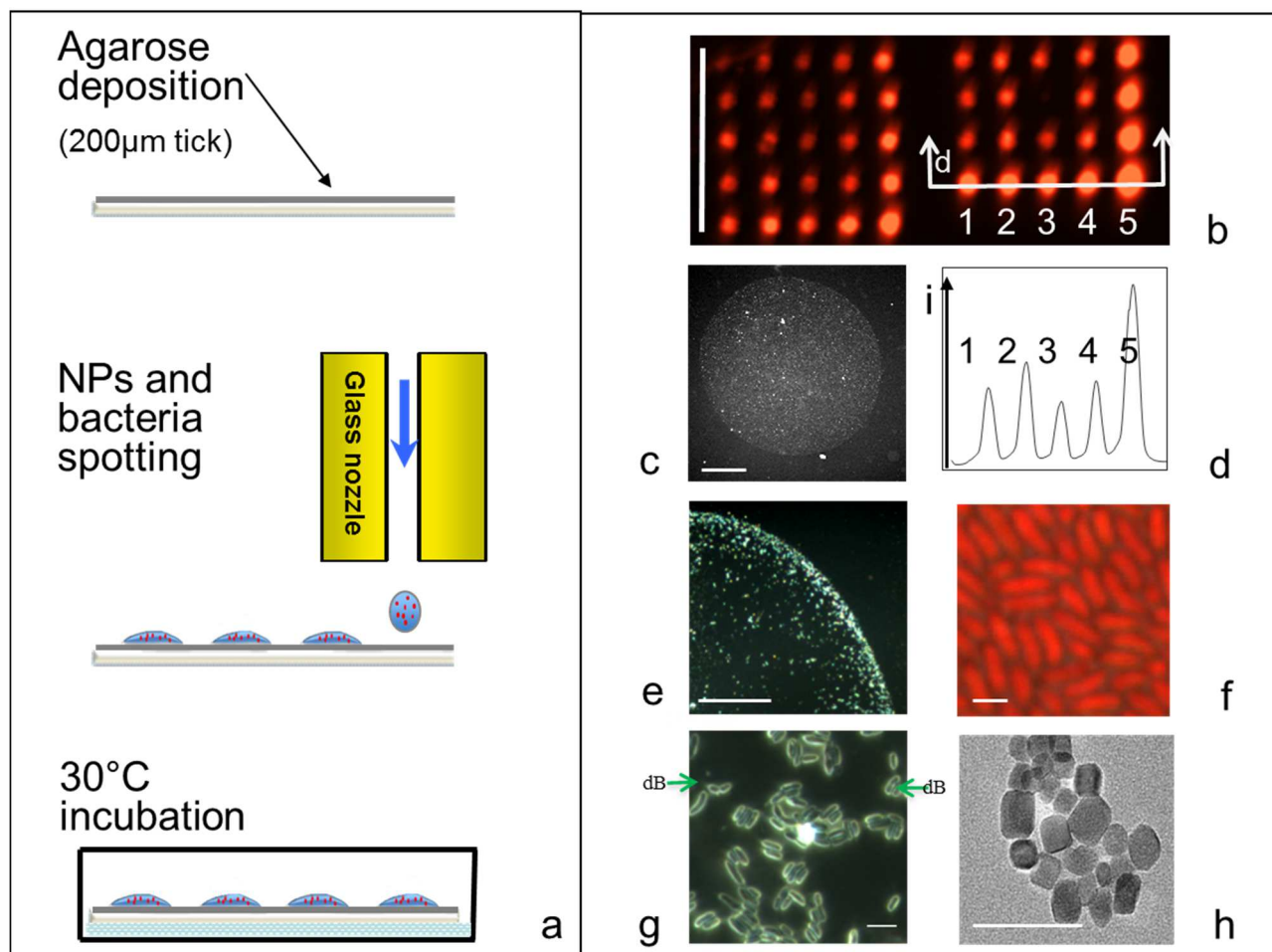


Fig. 1 The bacteria NP-biochip. **a.** Schematic showing the three fabrication steps, with plated glass slide (light grey), agarose containing the culture media (dark grey), drops (dark blue) containing NPs and bacteria (red); the picture at the bottom shows the plate as incubated in a Petri dish (black line) containing agar (light blue). **b.** Chemidoc imager scan of the NP-biochip comprising 50 spots with different types and amounts of NPs, after 48 h incubation, showing RFP expression; **c.** Microscope spot detail (550 nm, 20  $\times$ ) showing the fluorescent bacteria before incubation. **d.** Intensity profile along 5 spots noted 1 to 5 in scan b; **e. and g.** Hyperspectral images showing both GFP expressing *P. brassicacearum* strain NFM421 by fluorescence microscopy (green) and TiO<sub>2</sub> NPs (white) using 100  $\times$  magnification; **f.** RFP expressing *P. brassicacearum* strain NFM421 by fluorescence microscopy (550 nm, 100  $\times$ ); **h.** Transmission Electron Microscopy image of anatase NPs. Scale bars are: 10 mm (b), 100  $\mu$ m (c), 100  $\mu$ m (e), 1  $\mu$ m (f), 5  $\mu$ m (g), 100 nm (h). dB for dividing bacteria.

More details were obtained on a mixture-tuned matched filtering (MTMF) image resulting from hyperspectral image analysis of bacteria and TiO<sub>2</sub> NPs. The complete composite spectrum of each pixel in the visible and near-infrared wavelengths (400–1000 nm) was collected in a hyperspectral image (Fig. 2a). The spatial distribution and spectral information of NPs and bacteria were derived from each hyperspectral image using the Environment for Visualization ENVI v.4.4 software (Fig. 2b and c). Fig. 2a, b and c show, interestingly, that, at microscopic level, TiO<sub>2</sub> NPs do not prevent bacterial division, as was observed at

macroscopic level, although some bacterial cell surfaces appear to interact tightly with NPs. Indeed, hyperspectral imagery clearly indicates interaction between NPs and bacterial cell wall, combined with homo-aggregation of the NPs.

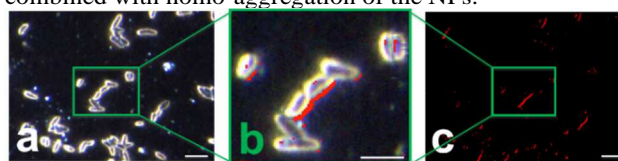


Fig. 2 Mixture Tuned Matched Filtering (MTMF) analysis of hyperspectral image. **a.** Collected hyperspectral image of a 20  $\mu\text{g/mL}$   $\text{TiO}_2$  NPs mixture (rutile, colored in red) and bacteria (white contours) on a NP-biochip spot, using  $100\times$  lens/1.3 oil iris; **b.** 4-fold zoom of a portion of the sample image (green rectangle area). **c.** The pixels matching the  $\text{TiO}_2$  NPs spectral library are colored in red, same view as in a. Scale bars are 5  $\mu\text{m}$  (a and c), 3  $\mu\text{m}$  (b).

### 3.2. Eukaryotic cell NP-biochip

The eukaryotic NP-biochip is well adapted to NP patterning in 100 dried matrigel® spots of 400  $\mu\text{m}$  diameter kept on a glass plate. Eucaryotic cells are too fragile to pass through a nozzle of comparable dimension (30 vs 80 $\mu\text{m}$ ) and could not be spotted. Therefore, the spotting and cell attachment were performed in two steps, according to Azioune et al.<sup>32</sup> (Fig. 3a). During the first step, one hundred hydrophilic 400  $\mu\text{m}$  wide spots containing NPs embedded in a cell-free matrix were formed on the glass plate rendered hydrophobic by a ultrathin layer of poly-L-lysine-grafted-polyethylene glycol coating. For this spotting, we used the dispense device and volume described above for the bacterial NP-biochip. We used the intrinsic fluorescence property of the matrigel to qualify matrix deposition in step 1. Fig. 3b and 3c illustrate that: the matrigel® matrix is precisely deposited; the dried spots present a rectangular profile and there is only a 0.3 % fluorescence variability in the matrix/NP amount. Similar reproducible profile was measured using QDs (not shown), in agreement with the literature<sup>38</sup>. The decorated glass plate was then immersed at 37 °C in a Petri dish containing the cells dispersed in 10 mL culture medium. This second step allowed precise positioning of cells on top of each NP/matrigel spot. The optimal duration of attachment (5 to 30 min) was shown to vary according to the cell type (data not shown, 10 min for 16-HBE cells). Several matrices (spotted in the first step, with the NPs) were tested: among them, matrigel®, a commercial mouse sarcoma-derived basement membrane protein mixture, at 6% w/v concentration, was shown to retain 44  $\pm$  10 adherent cells per spot. We have followed the product specification sheet in order to ensure homogeneity during pipetting.

The very good homogeneity of spot coverage by 16HBE cells, after two days of incubation at 37 °C allowing cell growth after step 2, is attested by Alexa Fluor® 488 phalloidin labeling in the microscopic view presented in Fig. 3d. Phalloidin is a high affinity filamentous actin probe revealing cell cytoplasm, and Alexa Fluor® 488 a fluorescent labeling allowing its quantitative detection. Using Rhodamine B - labelled NPs and QDs, we showed in Fig. 3e,f and Fig. 4 that NPs are able to diffuse from the solid phase to the cell membranes and get phagocytosed by the surrounding cells as already described by Alberola et al. and Simon-Deckers et al.<sup>39, 40</sup>. Interestingly, these authors and us, using different bronchial epithelial cell lines, reported that about 20 NP clusters per cell are formed after their translocation. This amount of clusters per cell is maintained on the whole chip, showing that the deposition and translocation processes are homogeneous on the whole chip surface. At macroscopic level, we used an alternate patterning of spots with and without QDs to check that NPs did not diffuse from spot to spot. Fig. 3e shows the cell nucleus in blue, as revealed by Hoechst 33342 nucleus coloration, and the QDs in red. On the one hand, there are definitely QDs inside the cells covering the QD spots. On the other hand, the QD-free spots are indeed covered by cells but devoid of QDs. At cell level, Fig. 3f and 4 show that the embedded  $\text{TiO}_2$  NPs, were able to leave the matrix and translocate into the adjacent eukaryotic cells.  $\text{TiO}_2$  NPs (shown in red) concentrated in vesicles, most probably lysosomes, in the cytoplasm (green). Here nucleus (blue) and actin (green) colorations are superimposed. Clearly the NPs have been translocated through the cell membrane and internalized in vesicles, as deduced from their defined clustered localization. The level of translocation was similar from cell to cell, as seen in Fig. 4b, most often around 20 round cytoplasmic vesicles per cell. Exceptionally, the level of translocation was much lower, as can be seen in Fig. 4a. We estimated a concentration of  $\text{TiO}_2$  NP in the order of 1 mg/mL in the cellular vesicles, by comparing the fluorescent intensity of the cellular vesicles with pure dried NP (not shown).

## ARTICLE

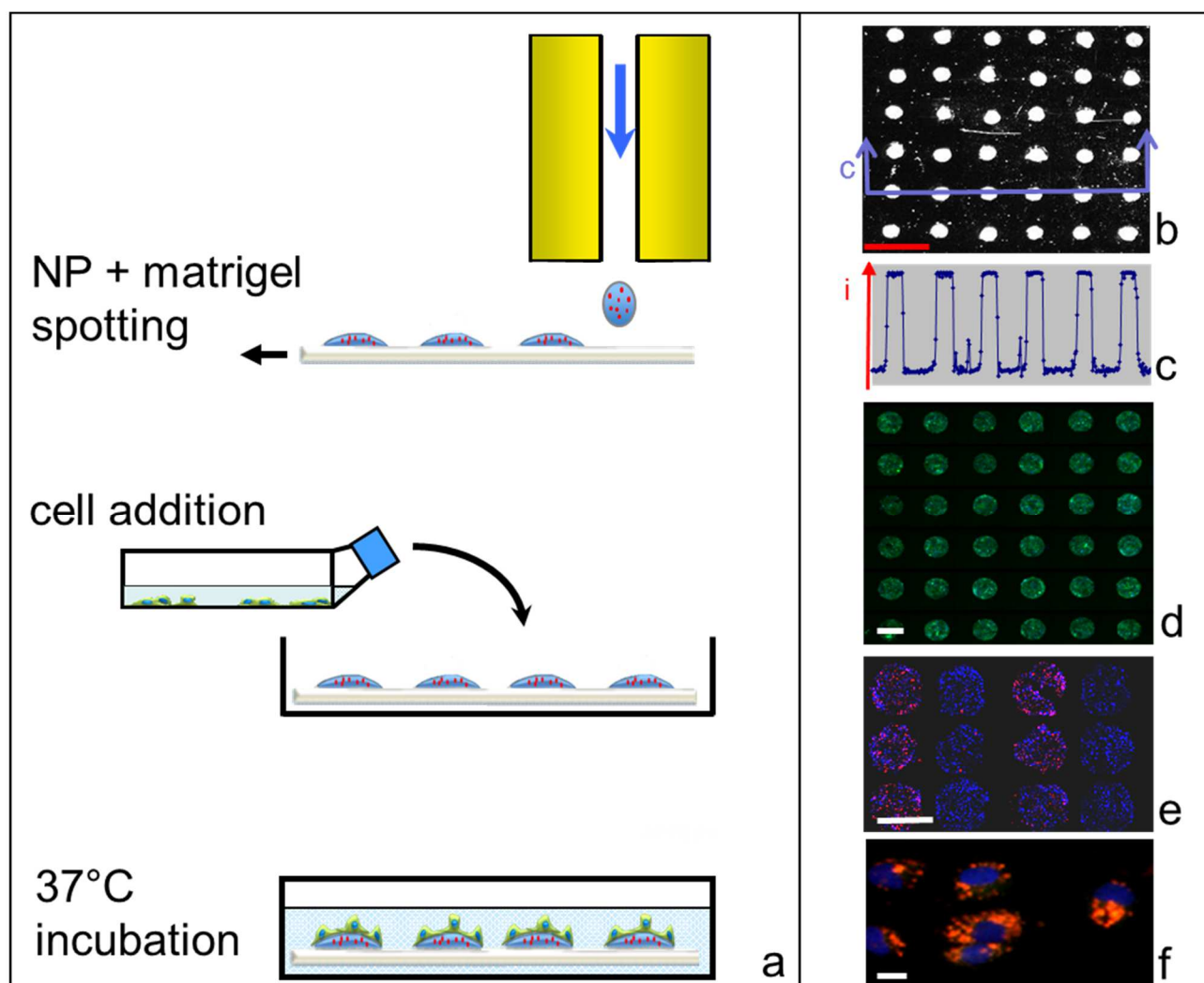


Fig. 3 The eukaryotic cell NP-biochip. **a.** Schematic of the automatic NP (red) and matrigel (dark blue) spotting followed by cell (green) attachment and 48 h growth with cell culture medium (light blue) incubated in a Petri dish (black line); **b.** Scan of the NP-biochip fluorescence after excitation at 550 nm before adding cells; **c.** Fluorescence profile of 6 spots from scan **b**; **d.** Microscope fluorescence imaging, 36 spot gallery of 16HBE bronchial cells, after cell attachment and 48 h incubation, detected by Alexa Fluor® 488 phalloidin labeling (10 × at 500 nm, green representation); **e.** Image gallery of 6 spots with 7 nm 'red' QDs and 6 spots without QDs, incubated with 16 HBE cells, nuclei are detected by Hoechst 33342 and appear in blue (10 ×, at 550 nm for QDs and at 360 nm for nucleus detection); **f.** Visualization of nucleus-labeled 16 HBE cells (blue) and rhodamine B - labeled 25 nm TiO<sub>2</sub> NP (red) (20 ×, at 550 nm for NP and at 360 nm for nucleus detection). Scale bars are 2 mm (b), 500 μm (d), 500 μm (e), 10 μm (f).

## ARTICLE

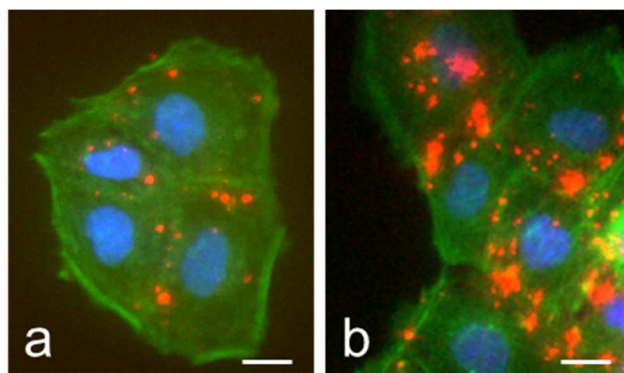


Fig. 4 NP-biochip reverse translocation in 16-HBE human bronchial epithelial cells after 48 h incubation with Rhodamine B – labeled (25 nm)  $\text{TiO}_2$  NPs. Microscopic views of two independent NP-biochips (a and b), the two images represent a range of translocation levels obtained from independent experiments. Fig. 4b representing the most common behavior. Superposition of fluorescent images captured at 550 nm for NPs detection (red), at 360 nm for nucleus detection (blue), and at 500 nm for actin detection (green) were obtained using a  $40\times$  lens. The beam was focused to image NP vesicles. Scale bar = 10  $\mu\text{m}$ .

#### 4. Discussion

A few years ago, we suggested using 100 nL drops, containing 100 cells each, to miniaturize cultures on a cell-on-chip substrate. This tool was successful in producing data, in particular  $\text{IC}_{50}$  measurements, describing toxicities (project TOXDROP granted by the European commission in FP6 program) in accordance with standard published data<sup>28</sup>. We developed in the present article a new concept which we called the ‘NP-biochip’, allowing bacteria and eukaryotic cell growth in the vicinity of NPs ( $\text{TiO}_2$  NPs or QDs), with technical specificities related to manipulation of each type of cells, here *P. brassicacearum* and human bronchial epithelial cells. Our device differed from the standard well procedure due to the fact that NPs were located under the cells, preventing sedimentation of NPs due to gravity. Analyses of NP effect on cell growth and NP/cell interactions were done using fluorescent bacteria or labeled eukaryotic cells and hyperspectral imaging. The release of nanomaterial from the matrix is an important aspect contributing to the success of a NP-biochip. A major observation in the present study was that both the QDs and the Rhodamine-labeled  $\text{TiO}_2$  samples appeared as aggregates in vesicles within the eukaryotic cells (Fig. 4) on the cell/NP-biochip; and as agglomerates on the bacterial membranes on the bacteria/NP-biochip (Fig. 2). Our observations showed that NPs released by the matrix of

the biochip entered the eukaryotic cells or became adherent to the bacterial membrane. Using classical culture, numerous studies have shown that NPs are indeed highly aggregated inside the cells in vesicles and in membranes<sup>20</sup> after incubation.

Hyperspectral imaging revealed that  $\text{TiO}_2$  NP accumulation at the bacterial surface did not prevent bacterial division. Fluorescence imaging using Rhodamine B - labeled  $\text{TiO}_2$  and QDs demonstrated in Fig. 4 their translocation into eukaryotic cells. The number of parallelized assays on biochips (50 or 100) allowed extensive NP *in vitro* toxicity medium throughput screening and thus could be used for evaluating health risks associated with NPs. Here we have considered only non-aggregated NPs, it would be interesting for future development to look at the effects of NP clusters and evaluate their evolution after interaction with bacteria or eukaryotic cells. NP-biochips may be relevant to study micro-organism and NP interactions in parallel assays. This new format could help test potential environmental impacts of NPs and perform nanoecotoxicology according to NP exposure.

The efficiency of this NP-biochip concept now needs to be evaluated. As a first example of assessment, Fig. 5a, shows the fluorescence intensity measurement of RFP bacteria incubated for 2 days on spots of the bacterial NP-biochip containing increasing concentrations of  $\text{TiO}_2$  anatase NP. It suggests that the reported membrane damages triggered by  $\text{TiO}_2$ <sup>10</sup> are not harmful enough to cause bacterial death in our experiment. We confirmed in Fig. 5b that this anatase  $\text{TiO}_2$  NP is innocuous by measuring the fluorescence intensity of RFP bacteria, incubated for 2 days in standard wells containing 200  $\mu\text{L}$  of TSB medium and increasing concentration of the same anatase  $\text{TiO}_2$  NP.

In a second example of assessment, quantitative evidence of the innocuous nature of an anatase  $\text{TiO}_2$  NP compared to the toxic nature of a rutile can also be found in Fig. 5c. The number of cells incubated on the eukaryotic cell NP-biochip containing increasing concentrations of the anatase or the rutile  $\text{TiO}_2$  NPs from Alfa Aesar was measured in duplicate experiments. In order to describe these NPs, Transmission Electron Microscopy (TEM) images are shown in Fig. 5e. Toxic effect of the rutile  $\text{TiO}_2$  NP was confirmed (Fig. 5f) by staining the spots of the chip with the fluorescent LIVE/DEAD® Cell Viability Assays. After 48h incubation, half of the cells were dead, as ascertained by red staining and half were alive, as ascertained by green staining. On the contrary, on non-toxic anatase  $\text{TiO}_2$  NP spots, no red signal corresponding to dead cell was found (data not shown).

## ARTICLE

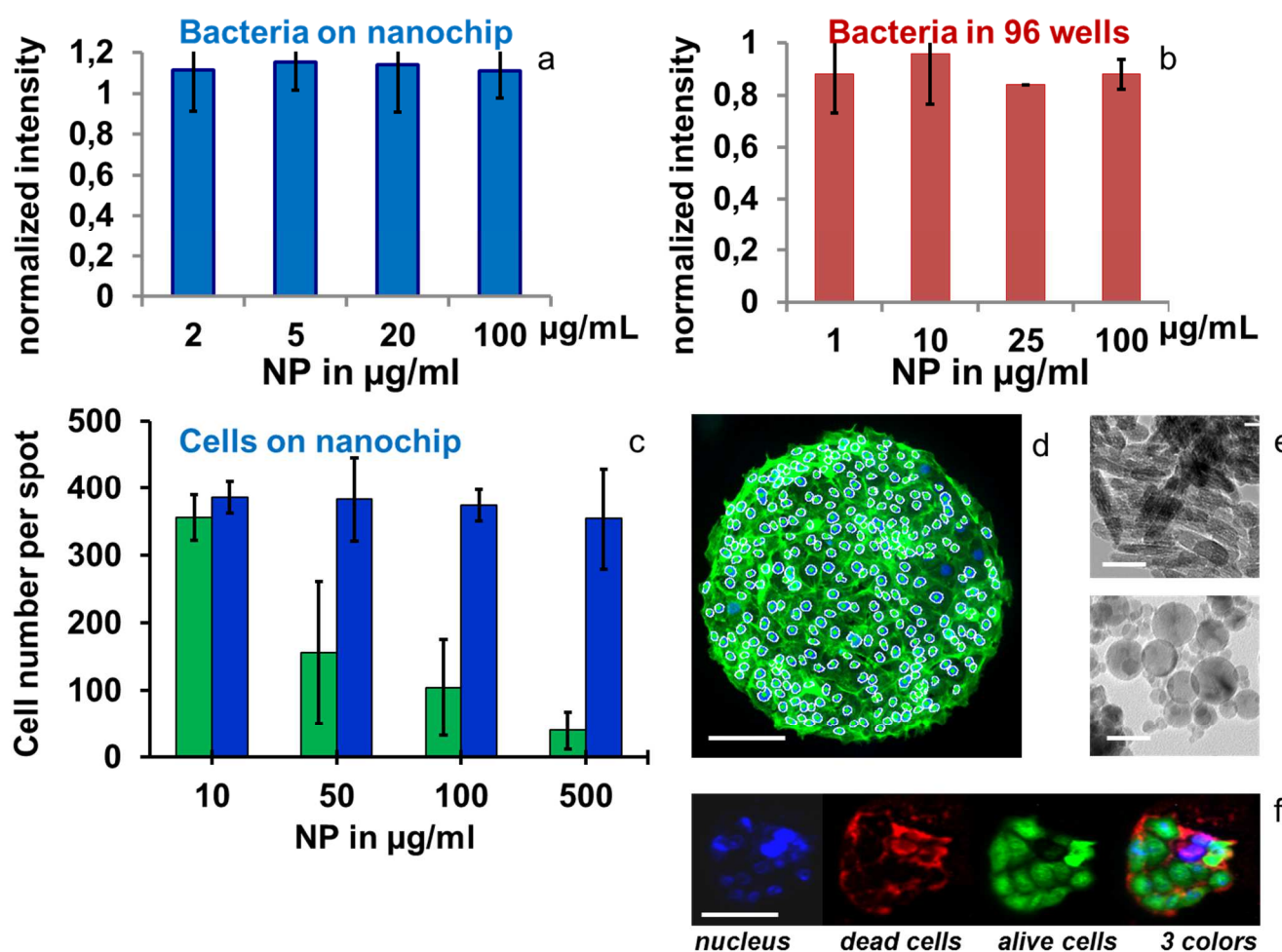


Fig. 5 Validation of the performance of the NP-biochip. **a.** Fluorescence intensity measurement of RFP bacteria incubated for 2 days on spots of the bacterial NP-biochip containing increasing concentrations of TiO<sub>2</sub> anatase NP. This value was normalized to the intensity measured on spots containing no NP (mean of: 5 spots for no NP, 6 spots for 2 mg/L, 5 spots for 5 mg/mL, 6 spots for 20 mg/L, 2 spots for 100 mg/L). The signal was captured using a Chemidoc MP imager and quantified using ImageLab software; **b.** Fluorescence intensity measurement of RFP bacteria incubated for 2 days in standard wells containing 200 µL of TSB medium for comparison with experiment a. Bacteria density (108 cells/mL) was estimated by serial dilution counting. Experiments were realized in quadruplicate; **c.** Numbers of cells incubated on the 16-HBE cell NP-biochip containing increasing concentrations of an anatase TiO<sub>2</sub> NP from Alfa Aesar (23 nm spheres, specific surface 44 m<sup>2</sup>/g) (blue bars) and a rutile TiO<sub>2</sub> NP from Alfa Aesar (47x18x18nm sticks, specific surface 45 m<sup>2</sup>/g) (green bars); experiments were realized in duplicate. Standard deviations are indicated for experiments a, b and c. The fluorescent data have been normalized in respect to the fluorescence measured in the absence of NPs; **d.** Cell counting for panel c, is illustrated on one spot by white circles drawn using ImageJ software around Hoechst® labeled nucleus; **e.** TEM images of anatase (bottom) and rutile (top) NPs used in c.; **f.** LIVE/DEAD® Cell Viability Assays on a 16-HBE cell NP-biochip containing 100 µg/mL of the toxic rutile TiO<sub>2</sub> NP used in c. Viable cells (shown in green) and dead cells (shown in red) were detected using Fluorescence Microscopy (ex/em 495 nm/515 nm) and (ex/em 495 nm/635 nm), respectively. Nucleus were stained using Hoechst® 33342. Scale bars are: 100 µm (d and f), 50 nm (e).

The NP-biochip should now be adaptable to numerous bacterial strains. The configuration of the NP-biochip for bacteria is convenient for testing physical, chemical, and genetic alterations. For either NP-biochip we did not here investigate

NP-media (matrigel or culture media) interactions, which could affect NP toxic effects<sup>41,42</sup>. We hope that this device, allowing the investigation of NP-bacteria interactions, may help correlate the physical-chemical properties of engineered TiO<sub>2</sub> NPs

according to their biological response and toxicity. The next step would be to undertake assays revealing cell response to NPs, in order to complement data on cell death described in this paper. Further studies are indeed underway to determine the impact of NPs on the expression of certain genes involved in iron metabolism and oxidant stress response. This is done by using constructs fusing the promoter of the genes of interest to fluorescent protein reporter genes<sup>43,44</sup>. NP-biochips would allow evaluating ncRNA (non-coding regulating RNA) expression related to oxidative stress and iron homeostasis in relation to different TiO<sub>2</sub> NPs or other NPs. In addition, the bacterial NP-biochip could be used to monitor biofilm formation in relation to the NP arrangement, using confocal laser scanning microscopy, which provides virtual optical sections with depth selectivity that can reveal the topology and 3-dimensional organization of cells expressing fluorescent RFP.

On the eukaryotic cell NP-biochip, the matrigel® can be considered as mimicking the physiological extracellular matrix of tissues within the human body. We have tested here the growth of pulmonary 16-HBE cell lines (*i.e.* cell number doubling per day), but intracellular responses (*i.e.* ROS production, cytokines quantification) of any adherent cell type could now be assessed and compared. It would permit to correlate cell behavior to NP physiological effects reported in animals: oxidative injury, inflammation, fibrosis, cytotoxicity, and release of pro-inflammatory mediators<sup>14</sup>. These medium throughput assays may help to solve the reported conflicting NP *in vitro* results<sup>17,18</sup>, which are likely to be the result of variations in experimental procedures. Fig. 5c shows the performance of the eukaryotic NP-biochips and analyses the effect of increasing concentrations of anatase and rutile TiO<sub>2</sub> NPs incubation over two days. A constant value of 407 +/- 57 16-HBE cells per spot was found for up to 500 µg/mL NPs on the NP-biochip, illustrating non-toxicity of an anatase TiO<sub>2</sub> NP in these conditions. On the contrary Fig. 5c and 5f illustrate the possible toxicity of a rutile TiO<sub>2</sub> NP. Understanding the mechanism of this toxicity is the subject of further studies.

## Conclusions

Over the last ten years, series of evaluations have helped define plausible human risk posed by NPs<sup>45-46</sup>. Coherence with European policy regarding nanotoxicology emerged from various collaborative research projects in which the Institute for Health and Consumer Protection (IHCP) is playing a key role today. European Guidelines have been implemented in order to test *in vitro* TiO<sub>2</sub> NPs used in cosmetics. Nanomaterial cytotoxicity<sup>17</sup> and chemical toxicity in the environment<sup>10</sup> were investigated according to NP composition and size, and shown to be cell-type dependent in eukaryotic cells as well as bacteria, but complementary studies remain to be done. *In vitro* studies are also needed to provide risk assessments in pathophysiology as well as in environmental studies. In addition, test standardization for NP safety evaluation requires multiple and repeated toxicity assays, using different cell types and different experimental conditions. Thus, new devices, easy to implement and with good performances, need to be elaborated for a large number of manufactured NP *in vitro* testing.

Kahru and Dubourguier<sup>10</sup> have stressed that nanosize materials have already been investigated *in situ* in animals, algae and soil communities in concentrations over 100 mg/L. The NP impact studies (as those planned in the international iCEINT project)

should now be conducted over longer periods of time, with diluted concentrations of NPs (below 200 µg/L<sup>47</sup>) in order to reveal the interaction of nanomaterial with living systems and their consequences, and to simulate the environment concentrations most often found in nature. Our preliminary experiments showed cell surviving up to three weeks on eukaryotic NP-biochips, provided the feeding culture medium is renewed, a process allowed by the biochip design. This is encouraging, but has to be optimized, to investigate chronic risks with low NP concentrations. From our results, it is not unrealistic to plan experiments with micro-organism-based NP-biochip and monitor the kinetic of NP internalization. The freshwater hydra, which is at the base of metazoan evolution, could be the first micro-organism to be targeted. This invertebrate model composed of two epithelial cell layers (an inner endoderm and an outer ectoderm facing the medium), simpler than vertebrates, has been shown to be an amenable system to study the interaction between NPs and organisms<sup>48,49</sup>.

## Acknowledgements

The authors gratefully acknowledge CNRS and CEA for funding the iCEINT (International Consortium for the Environmental Implications of NanoTechnology). Additional financial support was provided by the French National Research Agency (ANR P2N 2010 MESONNET Project, ANR NANOTRANS), AMIDEX project, the CEA Transverse Toxicology Program, ECCOREV FR and the Labex Serenade (n° ANR-11-LABX-0064) funded by the « Investissements d'Avenir » French Government program. The authors gratefully thank Aude Maguer for NPs preparation, Kinga Malinger for help in TEM images in Fig. 5, Peter Reiss for the donation of Quantum dots, Olivier Durupthy for his implication in the synthesis of original anatase nanoparticles, Sylvain Caillat for help in the NP spotting, Amandine Pitaval, Xavier Gidrol and Cécile Moro for their implication in the NP-biochip concept. We also thank Nayla Farouky and Remy Maximilien for valuable discussions.

## Notes and references

- <sup>a</sup> Univ. Grenoble Alpes, IBS, F-38044 Grenoble, France
- <sup>b</sup> CNRS, IBS, F-38044 Grenoble, France.
- <sup>c</sup> CEA, IBS, F-38044 Grenoble, France.
- <sup>d</sup> CEA, DSV, iRTSV, Laboratoire Biomics, F-38054 Grenoble, France.
- <sup>e</sup> CEA, DSV, IBEB, SBVME, Lab Ecol Microb Rhizosphere & Environ Extrem (LEMIRE), 13108 Saint-Paul-lez-Durance, France.
- <sup>f</sup> CNRS, UMR 6191, FR CNRS 3098 ECCOREV, 13108 Saint-Paul-lez-Durance, France.
- <sup>g</sup> Aix-Marseille Université, 13108 Saint-Paul-lez-Durance, France.
- <sup>h</sup> Institut Méditerranéen de Biodiversité et d'Ecologie marine et continentale, IMBE UMR-CNRS 7263, Aix-Marseille Université, Marseille, France.
- <sup>i</sup> CEA, Centre de Grenoble, DTNM/LSIN, 17 rue des Martyrs, 38054 Grenoble Cedex 9, France.
- <sup>j</sup> Centre des matériaux: Mines ParisTech, PSL Research University, Centre des Matériaux PM Fourt BP87 91003 Evry cedex.
- <sup>k</sup> ENSTA UCP SCPI, Université Paris-Saclay, 828 Bd des Maréchaux 91762 Palaiseau cedex France.
- <sup>l</sup> UPMC Univ Paris 06, CNRS, UMR 7574, Chimie de la Matière Condensée de Paris, Collège de France, 11 place Marcelin Berthelot, 75231 Paris Cedex 05, France.

<sup>m</sup> International Consortium for the Environmental Implications of Nano Technology, iCEINT, Europôle de l'Arbois, 13545 Aix en Provence, France

### Keywords:

Biochip, risk assessment, nanotoxicology, nanoecotoxicology

### References

- H. Shi, R. Magaye, V. Castranova and J. Zhao, *Part Fibre Toxicol*, 2013, **10**, 15.
- K. Donaldson, V. Stone, C. L. Tran, W. Kreyling and P. J. Borm, *Occupational and environmental medicine*, 2004, **61**, 727-728.
- A. S. Barnard, *Nature nanotechnology*, 2010, **5**, 271-274.
- J. Labille, J. Feng, C. Botta, D. Borschneck, M. Sammut, M. Cabie, M. Auffan, J. Rose and J. Y. Bottero, *Environ Pollut*, 2010, **158**, 3482-3489.
- Q. Li, S. Mahendra, D. Y. Lyon, L. Brunet, M. V. Liga, D. Li and P. J. Alvarez, *Water Res*, 2008, **42**, 4591-4602.
- F. R. Marciano, D. A. Lima-Oliveira, N. S. Da-Silva, A. V. Diniz, E. J. Corat and V. J. Trava-Airoldi, *J Colloid Interface Sci*, 2009, **340**, 87-92.
- The Project on Emerging Nanotechnologies. <http://www.nanotechproject.org>.
- J. Wu, W. Liu, C. Xue, S. Zhou, F. Lan, L. Bi, H. Xu, X. Yang and F. D. Zeng, *Toxicol Lett*, 2009, **191**, 1-8.
- N. Sadrieh, A. M. Wokovich, N. V. Gopee, J. Zheng, D. Haines, D. Parmiter, P. H. Siitonen, C. R. Cozart, A. K. Patri, S. E. McNeil, P. C. Howard, W. H. Doub and L. F. Buhse, *Toxicol Sci*, 2010, **115**, 156-166.
- A. Kahru and H. C. Dubourguier, *Toxicology*, 2010, **269**, 105-119.
- B. Trouiller, R. Reliene, A. Westbrook, P. Solaimani and R. H. Schiestl, *Cancer Res*, 2009, **69**, 8784-8789.
- C. Monteiller, L. Tran, W. MacNee, S. Faux, A. Jones, B. Miller and K. Donaldson, *Occup Environ Med*, 2007, **64**, 609-615.
- A. S. Yazdi, G. Guarda, N. Riteau, S. K. Drexler, A. Tardivel, I. Couillin and J. Tschopp, *Proceedings of the National Academy of Sciences of the United States of America*, 2010, **107**, 19449-19454.
- G. Oberdorster, E. Oberdorster and J. Oberdorster, *Environ Health Perspect*, 2005, **113**, 823-839.
- S. Novak, D. Drobne, J. Valant, Z. Pipan-Tkalec, P. Pelicon, P. Vavpetic, N. Grlj, I. Falnoga, D. Mazej and M. Remskar, *Environmental Toxicology and Chemistry*, 2012, **31**, 1083-1090.
- T. R. Nurkiewicz, D. W. Porter, A. F. Hubbs, S. Stone, A. M. Moseley, J. L. Cumpston, A. G. Goodwill, S. J. Frisbee, P. L. Perrotta, R. W. Brock, J. C. Frisbee, M. A. Boegehold, D. G. Frazer, B. T. Chen and V. Castranova, *Res Rep Health Eff Inst*, 2011, 3-48.
- S. K. Sohaebuddin, P. T. Thevenot, D. Baker, J. W. Eaton and L. Tang, *Part Fibre Toxicol*, 2010, **7**, 22.
- J. Valant, I. Iavicoli and D. Drobne, *Protoplasma*, 2012, **249**, 493-502.
- W. Jiang, K. Yang, R. W. Vachet and B. S. Xing, *Langmuir : the ACS journal of surfaces and colloids*, 2010, **26**, 18071-18077.
- S. Singh, T. Shi, R. Duffin, C. Albrecht, D. van Berlo, D. Hohr, B. Fubini, G. Martra, P. Fenoglio, P. J. Borm and R. P. Schins, *Toxicology and applied pharmacology*, 2007, **222**, 141-151.
- A. Kumar, A. K. Pandey, S. S. Singh, R. Shanker and A. Dhawan, *Free radical biology & medicine*, 2011, **51**, 1872-1881.
- Environmental, Health, And Safety Research Strategy. [http://nano.gov/sites/default/files/pub\\_resource/nni\\_2011\\_ehs\\_research\\_strategy.pdf](http://nano.gov/sites/default/files/pub_resource/nni_2011_ehs_research_strategy.pdf).
- D. A. Pelletier, A. K. Suresh, G. A. Holton, C. K. McKeown, W. Wang, B. Gu, N. P. Mortensen, D. P. Allison, D. C. Joy, M. R. Allison, S. D. Brown, T. J. Phelps and M. J. Doktycz, *Applied and environmental microbiology*, 2010, **76**, 7981-7989.
- I. G. de Jong, J. W. Veening and O. P. Kuipers, *Environ Microbiol*, 2012, **14**, 3110-3121.
- P. Ortet, M. Barakat, D. Lalaouna, S. Fochesato, V. Barbe, B. Vacherie, C. Santaella, T. Heulin and W. Achouak, *Journal of bacteriology*, 2011, **193**, 3146.
- W. Achouak, L. Sutra, T. Heulin, J. M. Meyer, N. Fromin, S. Degraeve, R. Christen and L. Gardan, *International journal of systematic and evolutionary microbiology*, 2000, **50 Pt 1**, 9-18.
- X. Gidrol, B. Fouque, L. Ghenim, V. Haguët, N. Picollet-D'hahan and B. Schaack, *Current opinion in pharmacology*, 2009, **9**, 664-668.
- F. Lemaire, C. A. Mandon, J. Reboud, A. Papine, J. Angulo, H. Pointu, C. Diaz-Latoud, C. Lajaunie, F. Chatelain, A. P. Arrigo and B. Schaack, *PloS one*, 2007, **2**, e163.
- W. Achouak, S. Conrod, V. Cohen and T. Heulin, *Molecular plant-microbe interaction. : MPMI*, 2004, **17**, 872-879.

30. A. Dessombz, D. Chiche, P. Davidson, P. Panine, C. Chaneac and J. P. Jolivet, *Journal of the American Chemical Society*, 2007, **129**, 5904-5909.
31. A. M. Merendino, C. Paul, A. M. Vignola, M. A. Costa, M. Melis, G. Chiappara, V. Izzo, J. Bousquet and A. P. Arrigo, *Cell Stress Chaperones*, 2002, **7**, 269-280.
32. A. Azioune, M. Storch, M. Bornens, M. They and M. Piel, *Lab Chip*, 2009, **9**, 1640-1642.
33. D. Castel, M. A. Debily, A. Pitaval and X. Gidrol, *Methods Mol Biol*, 2007, **381**, 375-384.
34. A. Pitaval, Q. Tseng, M. Bornens and M. They, *The Journal of cell biology*, 2010, **191**, 303-312.
35. M. Protiere, N. Nerambourg, O. Renard and P. Reiss, *Nanoscale research letters*, 2011, **6**, 472.
36. A. R. Badireddy, M. R. Wiesner and J. Liu, *Environmental science & technology*, 2012, **46**, 10081-10088.
37. B. Khoobehi, J. M. Beach and H. Kawano, *Investigative ophthalmology & visual science*, 2004, **45**, 1464-1472.
38. E. V. Ushakova, A. P. Litvin, P. S. Parfenov, A. V. Fedorov, M. Artemyev, A. V. Prudnikau, I. D. Rukhlenko and A. V. Baranov, *ACS nano*, 2012, **6**, 8913-8921.
39. A. P. Alberola and J. O. Radler, *Biomaterials*, 2009, **30**, 3766-3770.
40. A. Simon-Deckers, B. Gouget, M. Mayne-L'hermite, N. Herlin-Boime, C. Reynaud and M. Carriere, *Toxicology*, 2008, **253**, 137-146.
41. M. P. Monopoli, D. Walczyk, A. Campbell, G. Elia, I. Lynch, F. B. Bombelli and K. A. Dawson, *Journal of the American Chemical Society*, 2011, **133**, 2525-2534.
42. W. Liu, J. Rose, S. Plantevin, M. Auffan, J. Y. Bottero and C. Vidaud, *Nanoscale*, 2013, **5**, 1658-1668.
43. D. Lalaouna, S. Fochesato, M. Barakat, P. Ortet and W. Achouak, *Journal of bacteriology*, 2012, **194**, 4888-4893.
44. D. Lalaouna, S. Fochesato, L. Sanchez, P. Schmitt-Kopplin, D. Haas, T. Heulin and W. Achouak, *Applied and environmental microbiology*, 2012, **78**, 1658-1665.
45. C. M. Sayes, R. Wahi, P. A. Kurian, Y. Liu, J. L. West, K. D. Ausman, D. B. Warheit and V. L. Colvin, *Toxicological sciences : an official journal of the Society of Toxicology*, 2006, **92**, 174-185.
46. Q. Rahman, M. Lohani, E. Dopp, H. Pemsel, L. Jonas, D. G. Weiss and D. Schiffmann, *Environmental health perspectives*, 2002, **110**, 797-800.
47. T. Y. Sun, F. Gottschalk, K. Hungerbuhler and B. Nowack, *Environ Pollut*, 2014, **185**, 69-76.
48. V. Marchesano, Y. Hernandez, W. Salvenmoser, A. Ambrosone, A. Tino, B. Hobmayer, J. M. de la Fuente and C. Tortiglione, *ACS nano*, 2013, **7**, 2431-2442.
49. C. Tortiglione, A. Quarta, M. A. Malvindi, A. Tino and T. Pellegrino, *PLoS one*, 2009, **4**.